

## Seasonality of Large-Scale Atmosphere–Ocean Interaction over the North Pacific

YUAN ZHANG, JOEL R. NORRIS,\* AND JOHN M. WALLACE

*Department of Atmospheric Sciences, University of Washington, Seattle, Washington*

(Manuscript received 14 July 1997, in final form 1 December 1997)

### ABSTRACT

This paper attempts to resolve a long-standing paradox concerning the season-to-season memory of sea surface temperature anomalies (SSTAs) over the North Pacific. Summertime SSTAs are confined to a shallow mixed layer that is obliterated by wind-driven mixing in late autumn or early winter storms. The mixing exposes waters that were last in contact with the surface during the previous spring. Hence, SSTAs at fixed locations exhibit little memory from summer to the next winter. Yet despite this apparent lack of memory, a well-defined pattern of summertime and autumn SSTAs exhibits significant correlations with the sea level pressure field over the North Pacific a season later.

It is shown that the dominant mode of SSTA variability over the North Pacific, as inferred from empirical orthogonal function (EOF) analysis, exhibits a rather similar spatial structure year-round, with highest amplitude during summer. By means of singular value decomposition analysis, it is shown that this pattern is much more persistent from one season to the next (and particularly from summer to the next winter) than SSTAs at fixed grid points. It is substantially more persistent from one summer to the next than from one winter to the next, reflecting the relatively greater prominence of the interdecadal variability in the summertime SSTAs.

The minor differences in the structure of the winter and summer EOFs can be attributed to the coupling with the atmospheric Pacific North American pattern during winter, which induces SSTAs off the west coast of North America opposite in polarity to those in the central and western Pacific.

### 1. Introduction

Sea surface temperature anomalies (SSTAs) over the North Pacific exhibit a remarkable amount of persistence from one year to the next, as reflected in the strong interdecadal variability of the leading EOF (e.g., see Zhang et al. 1997). Just how these long-term fluctuations come about, and how SSTAs of the same polarity are sustained year after year in the presence of random atmospheric variability, ENSO-related interannual variability, and large seasonal variations in the structure of the oceanic mixed layer, is not well understood.

In their seminal paper on the temporal persistence of sea surface temperature, Namias and Born (1970, hereafter NB) showed evidence that the month-to-month autocorrelation of SSTAs drops off more gradually during the cold season. They attributed the higher wintertime persistence to the greater depth and thermal inertia of the oceanic mixed layer during winter: a consequence of the stronger surface winds and the more vigorous

vertical mixing. Their autocorrelation functions for SSTAs starting from the cold season exhibit minor peaks for lags around 12 and 24 months, suggestive of a recurrence of SSTAs in successive winters. They attributed this feature to the “storage of anomalously cold or warm water that is shielded by a shallow layer in summer but is stirred up to the surface by the increased wind stress during cold months.” The seasonality of the autocorrelation statistics noted by NB has been corroborated by the subsequent studies of Walsh and Richman (1981) and Wallace and Jiang (1987), and the interpretation that they offered is supported by the results of Alexander and Deser (1995), who examined monthly mean SST and subsurface temperature data from ocean weather ships P and N in the eastern Pacific. Simultaneous correlations between SST and subsurface temperature anomalies (their Fig. 4) clearly illustrate the decoupling of the shallow summertime mixed layer from the temperature anomalies at depth, and lead/lag correlations (their Fig. 6) indicate that the anomalies at depth during summer are linked to temperature anomalies extending through the mixed layer during the previous and subsequent cold seasons.

Because of their stronger persistence and their stronger coupling with the atmospheric geopotential height field, SSTAs during the cold season have been the focus of most of the research on large-scale extratropical atmosphere–ocean interaction. Works of Kawamura

---

\* Current affiliation: National Center for Atmospheric Research, Boulder, Colorado.

---

Corresponding author address: Joel R. Norris, NCAR/ASP, P.O. Box 3000, Boulder, CO 80307-3000.  
E-mail: jnorris@ucar.edu

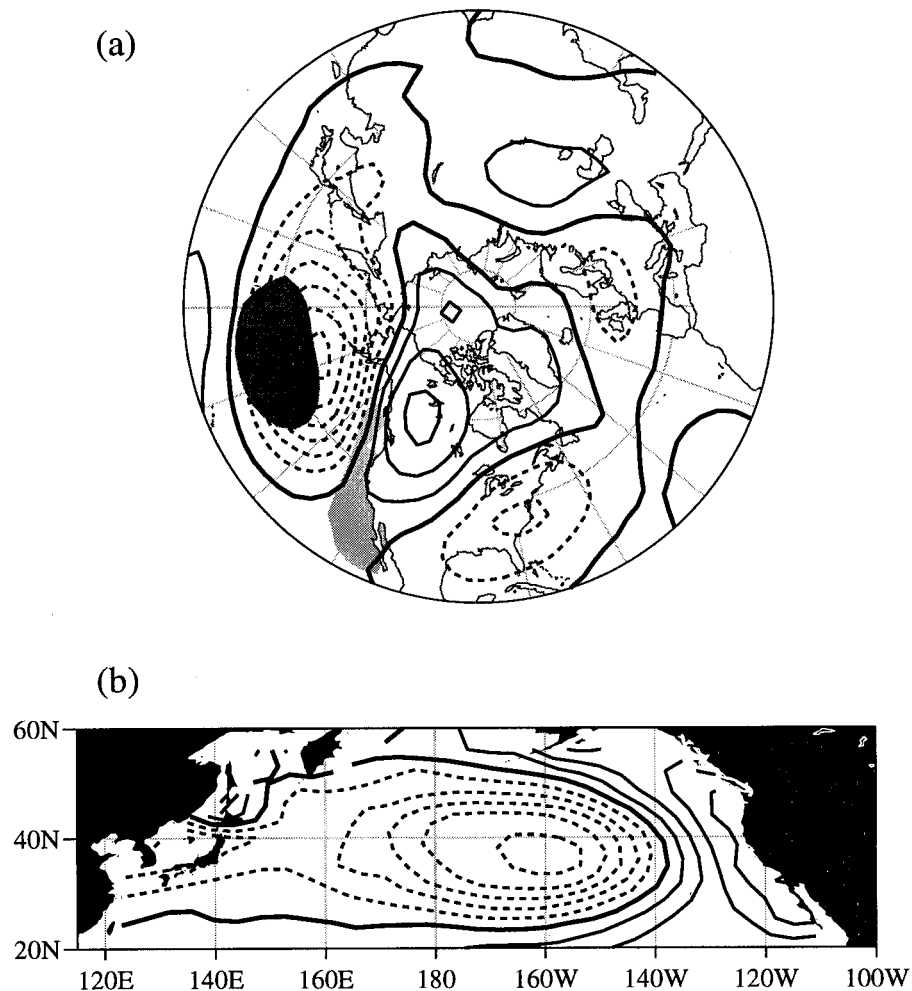


FIG. 1. The leading wintertime mode of coupled year-to-year variability in (a) the hemispheric 500-mb height field and (b) North Pacific SST as inferred from SVD analysis of seasonal-mean (Dec–Feb) fields. The contoured values were obtained by regressing the 500-mb height field upon the normalized expansion coefficient time series of SST and vice versa. The SCF/ $r$ /NC for this mode are 0.68/0.84/0.20, compared to 0.37/0.63/0.10 for its summertime counterpart (not shown). The contour interval is 10 m for 500-mb height and 0.1 K for SST; the zero contour is thickened and negative contours are dashed. Shading in (a) shows the placement of the major centers of action in (b).

(1984), Cayan, (1992a,b), and Iwasaka and Wallace (1995) have shown how wintertime SSTAs, generated primarily through the latent and sensible heat fluxes at the air–sea interface, exhibit spatially coherent patterns in association with large-scale atmospheric circulation anomalies. As illustrated in Fig. 1, an SST pattern virtually indistinguishable from the leading EOF of the wintertime SST field (Davis 1976) is coupled with the atmosphere’s dominant mode of low-frequency variability in this sector, the Pacific–North American (PNA) pattern. The observational evidence indicates that the SST perturbations are a forced response to fluctuations in the atmospheric circulation (Frankignoul 1985), and numerical simulations with atmospheric models forced by prescribed SSTAs indicate that SSTAs, in turn, are capable of exerting a discernible influence upon the at-

mospheric circulation (e.g., Ferranti et al. 1994). Simulations with coupled atmosphere–ocean models suggest that two-way interactions involving the PNA pattern and the leading EOF of wintertime SSTAs might be a major source of interdecadal-scale climate variability over the North Pacific (Latif and Barnett 1994; Yukimoto et al. 1996).

The role of summertime SSTAs in this scenario is not clear. The interactions described in the previous paragraph are not likely to be as important because the summertime atmospheric circulation anomalies are much weaker (e.g., see Wallace et al. 1993, their Fig. 1) and the PNA pattern is not a particularly prominent mode of summertime variability. Furthermore, the results of NB and Alexander and Deser (1995) could be interpreted as indicating that whatever thermal anom-

alies may have developed in the shallow summertime mixed layer are obliterated by vertical mixing in late autumn or early winter storms. Hence, it might be tempting to conclude that insofar as interannual or interdecadal climate variability is concerned, summertime SSTAs are largely irrelevant: the winter-to-winter memory of the coupled atmosphere–ocean patterns resides in the subsurface thermal anomalies.

The weight of evidence in support of NB’s “re-emergence hypothesis” invites the inference that warm season SSTAs over the extratropical North Pacific should not be significantly correlated with circulation anomalies over the Pacific sector during the following cold season, yet there is evidence to the contrary. In Davis’s (1978) search for statistical relationships that might have predictive value for North America, the most significant lag correlations that emerged were the ones for predicting autumn and winter sea level pressure (SLP) from the previous season’s SST. In both cases, SSTAs along 35°N in the western and central Pacific in the prior season appear to be related to PNA-like SLP anomalies a season or two later. Since the spatial patterns and polarities identified by Davis are very similar to the contemporaneous wintertime relationship depicted in Fig. 1, his results suggest, in apparent contradiction to the reemergence hypothesis, that summertime SSTAs in this region have a tendency to persist into the following autumn and winter seasons. The contradiction may be only an apparent one because NB did not actually consider the persistence of SST patterns: the autocorrelation statistics that they showed were calculated for local SSTAs and then averaged over a large number of individual grid points. It is conceivable that the behavior of SST patterns could be quite different. Indeed, if the ~4-month decorrelation time of local SSTAs, as deduced from observations and mixed layer models (Frankignoul 1985; Alexander 1992) were representative of the persistence of SST patterns, it would be difficult to account for the pronounced interdecadal variability of the leading EOF of North Pacific SST.

In view of the unresolved issues concerning the seasonality of SSTAs, there is scope for further investigation of the seasonality and persistence of SST patterns over the North Pacific. Of particular interest is the question of whether the dominant pattern of SSTAs persists from winter to the next summer and from summer to the next winter and, if so, whether it undergoes a systematic evolution with the change of the seasons. It will also be of interest to determine whether the dominant summertime pattern is as persistent, from one year to the next, as its wintertime counterpart. The results of this investigation will lead us to consider, in a companion paper (Norris et al. 1998), whether low cloudiness might play a significant role in summertime air–sea interaction over the North Pacific.

## 2. Data and analysis techniques

The analysis in this paper is based upon the trimmed version of the Comprehensive Ocean–Atmosphere Data

Set, as described in Fletcher et al. (1983) for the period June 1950–February 1994. The data were aggregated into 4° lat × 6° long boxes centered at 4°, 8°, 12°N, etc., and 177°E, 177°W, 171°W, etc. Most of the calculations were checked by performing them independently on the Global Ocean Surface Temperature Atlas dataset (Bottomley et al. 1990). The 500-mb height fields used in the preparation of Fig. 1 are based on the operational analyses of the U.S. National Centers for Environmental Prediction, formerly the National Meteorological Center, preprocessed as described in Kushnir and Wallace (1989).

The analysis tools used in this study are conventional EOF analysis and singular value decomposition (SVD), both of which are based on temporal covariance matrices. For a tutorial on SVD, the reader is referred to Bretherton et al. (1992). The squared covariance fraction (SCF) discussed extensively in Bretherton et al. is useful for comparing the relative importance of modes in a given expansion, but it is of limited value in comparing the strength of the relationship between the left and right fields in modes obtained from different SVD expansions, in which the squared covariance between the left and right fields may be much different. A useful supplementary statistic that provides a more direct comparison is the normalized root-mean-square covariance

$$NC_k = \frac{\pi_k^2}{\sqrt{\left(\sum_i \sigma_i^2\right)\left(\sum_j \sigma_j^2\right)}},$$

where  $k$  refers to the mode number,  $\pi_k^2$  is the square of the associated singular value and the squared covariance explained by that mode, and  $\sigma_i^2$  and  $\sigma_j^2$  are the variances at the  $i$ th grid point in the left field and the  $j$ th grid point in the right field. In this paper we will present SCF and NC for the leading mode in the various expansions, together with  $r$ , the correlation coefficient between the expansion coefficient time series of the left and right fields.

In presenting results of both EOF and SVD analysis, the patterns shown are derived by regressing the SST field upon the appropriate normalized expansion coefficient time series. Hence, the contoured values represent typical amplitudes of the fluctuations associated with that mode. In the terminology of Bretherton et al. (1992) the fields presented from SVD analysis are heterogeneous regression (or covariance) patterns.

In all area averages, and in all EOF and SVD analyses, variances and covariances are weighted by cosine of latitude so that equal areas carry equal weights.

## 3. Results

Figure 2 shows the distribution of the temporal standard deviation of wintertime (December–February; DJF) and summertime (June–August; JJA) mean SST. It is evident that the interannual variability of SST over

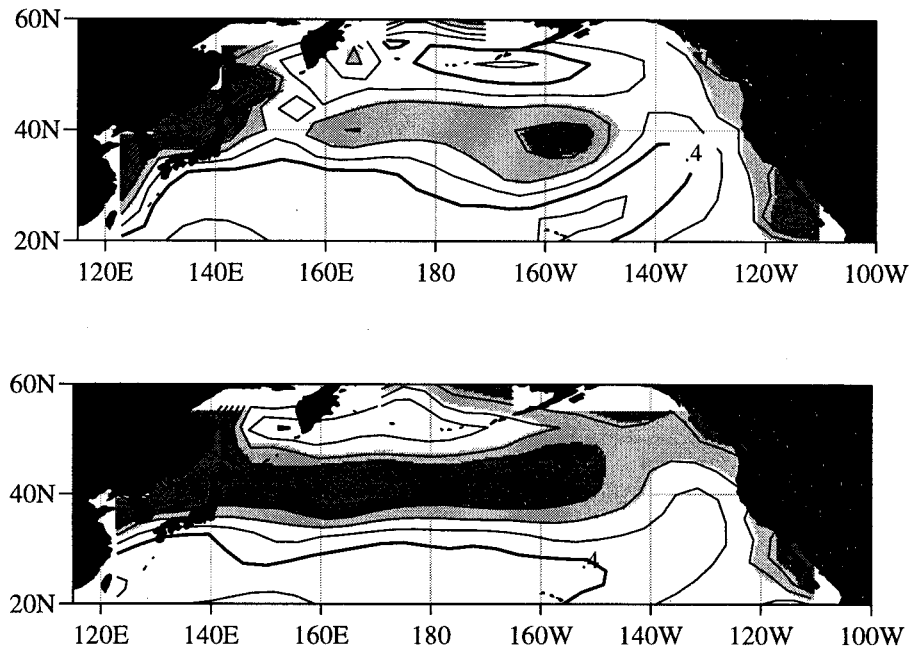


FIG. 2. Standard deviations of (top) wintertime (DJF), and (bottom) summertime (JJA) SST based on the period 1950–93. The contour interval is 0.1 K; the thickened contour corresponds to 0.4 K; thresholds for lighter (darker) shading are 0.6 (0.7) K.

most of the North Pacific tends to be slightly larger during summer. The patterns for the two seasons are similar, but the zone of highest variance along 40°N (indicated by the shading) is more zonally elongated and displaced slightly poleward during summer. Figure 3 shows the annual march of the root-mean-square variance of SST, averaged over the Pacific basin poleward of 18°N, together with the square root of the leading eigenvalue of SST for the same domain. Both exhibit relatively weak summertime maxima.

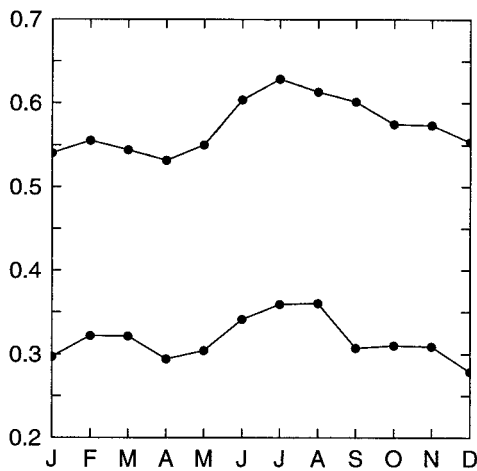


FIG. 3. Annual march of (top) the standard deviation of monthly mean SST, averaged over the North Pacific poleward of 18°N; and (bottom) the square root of the leading eigenvalue of the monthly mean SST field for the same region and period of record, both in units of K.

The leading EOFs of seasonal mean wintertime and summertime SSTAs over the North Pacific poleward of 18°N are shown in Fig. 4. The patterns for the two seasons are rather similar and account for roughly comparable amounts of variance; that is, the summer mode accounts for a slightly smaller fraction (29% vs 32%) of the variance, but the associated eigenvalue is larger (Fig. 3), owing to the larger variability of summertime SST. As in the variance field, the primary center of action in the summertime pattern is more zonally elongated and displaced slightly poleward in summertime. The secondary center of action along the west coast of North America is more prominent in the wintertime pattern.

The corresponding winter and summer principal components (PCs), shown in Fig. 4, exhibit remarkably similar patterns of interannual and interdecadal variability. The corresponding 1-yr lag correlations are 0.33 for wintertime and 0.47 for summertime. Hence, on the basis of this cursory analysis, the summertime variability does not appear to be any weaker, or any less coherent in space or in time than the wintertime variability. Now let us examine the season-to-season persistence.

The next two figures show the leading modes derived from SVD analysis of the SSTA field in successive seasons: winter paired with the following summer (Fig. 5) and summer paired with the following winter (Fig. 6). Summary statistics are presented in Table 1. In both cases the dominant features in the pattern for the later season are displaced eastward relative to their counterparts in the prior season. The implied eastward phase

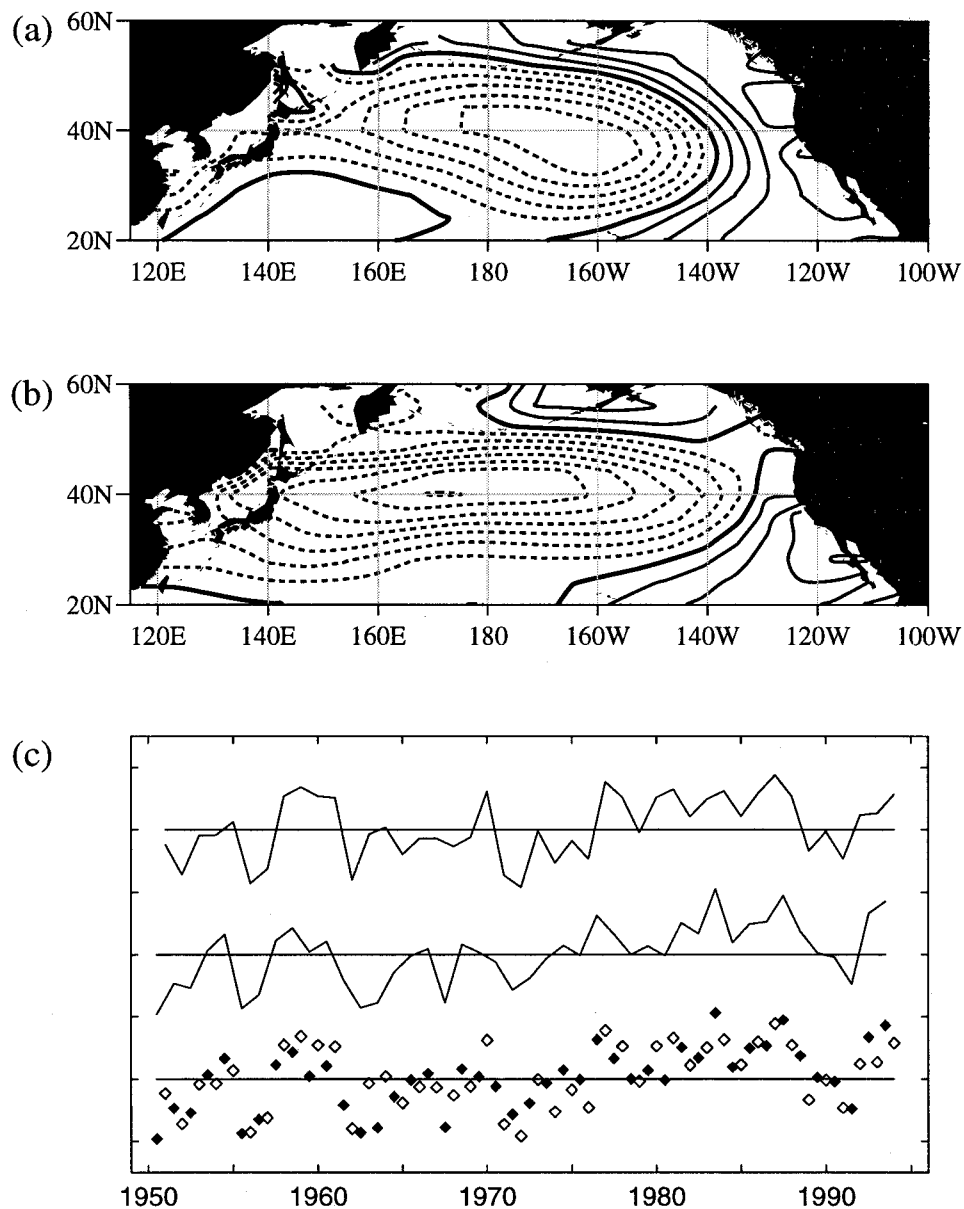


FIG. 4. Leading EOFs of the (a) wintertime and (b) summertime seasonal mean SST fields poleward of  $18^{\circ}\text{N}$ , scaled as described in section 2. The contour interval is  $0.1\text{ K}$ : the zero contour is thickened and negative contours are dashed. The corresponding normalized PC time series are shown in (c) for (top) wintertime, (middle) summertime, and (bottom) wintertime (open diamonds) and summertime (filled diamonds) together. Tick marks on the ordinate scale are at intervals of two standard deviations.

speed is on the order of  $10\text{ cm s}^{-1}$ , consistent with results of previous studies of Namias (1959) and Frankignoul (1985). Yet despite the apparent propagation, the patterns in Figs. 5 and 6 resemble the corresponding leading EOFs (Fig. 4): their spatial structures are similar and their expansion coefficients are correlated with the corresponding principal components at levels in excess of 0.95. The correlation coefficients between the wintertime and summertime expansion coefficient time series (0.69 for winter to summer and 0.75 for summer-to-winter) are far higher than the season to season cor-

relations reported by NB, based on monthly gridpoint data. The patterns and correlations are virtually unchanged when the analysis was repeated with the summer months defined as August–October instead of June–August (not shown).

The eastward propagation implied by the season to season displacements of the features in Figs. 5 and 6 is far too rapid to be relevant to the evolution of SSTA patterns on the interdecadal timescale and it is not as clearly apparent in SVD analyses of SSTA fields separated by a full year (not shown). It can be eliminated

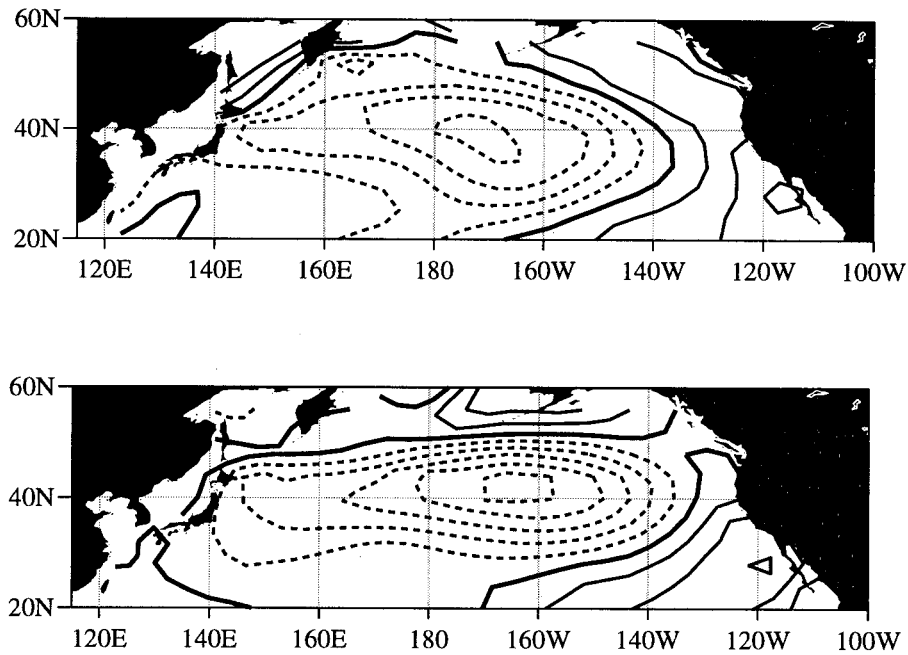


FIG. 5. Leading SVD mode for (top) wintertime SST paired with (bottom) SST for the following summer. The contour interval is 0.1 K; the zero contour is thickened and negative contours are dashed. Summary statistics are presented in Table 1.

by performing the SVD analysis in a manner analogous to centered finite differencing, with SSTA fields averaged for pairs of successive winter seasons paired with the SSTAs field for the intervening summer. Alternatively,

the analysis can be performed with fields for successive summers paired with the field for the intervening winter. We will refer to the former as WSW and the latter as SWS. The analogous winter paired with the

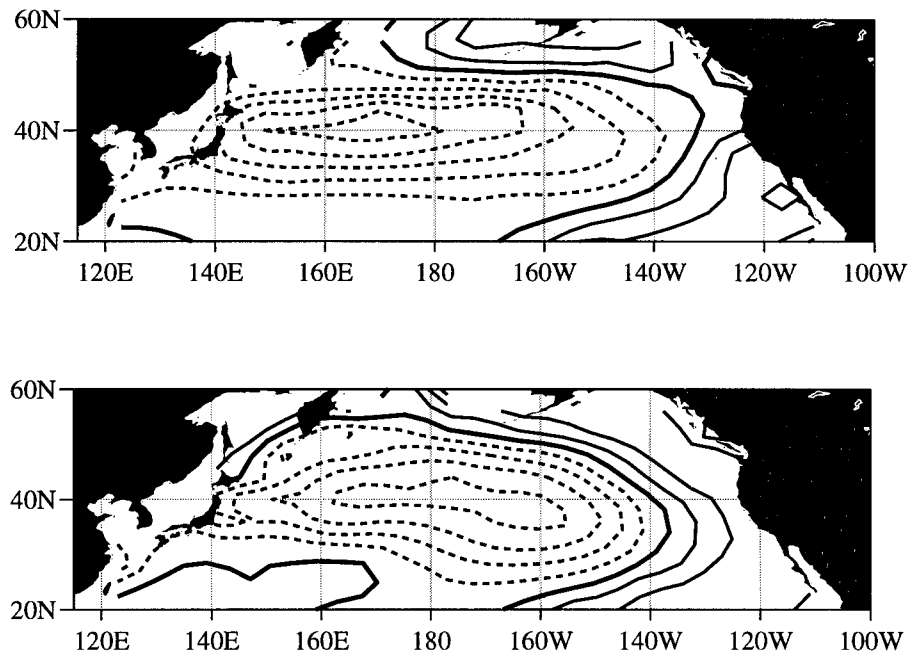


FIG. 6. Leading SVD mode for (top) summertime SST paired with (bottom) SST for the following winter. The contour interval is 0.1 K; the zero contour is thickened and negative contours are dashed. Summary statistics are presented in Table 1.

TABLE 1. Summary statistics for SVD analyses of SSTAs over the North Pacific poleward of 18°N: WS represents winter paired with the following summer; SW represents summer paired with the following winter.

	SCF	NC	<i>r</i>
WS	63	18	69
SW	65	21	75

average of previous and subsequent winters (WWW) results document the relationships between wintertime SST patterns and those in the prior and subsequent winter seasons, and similarly for the summers paired with the previous and subsequent summers (SSS). The patterns derived from these analyses are not shown because they all closely resemble the respective wintertime and summertime EOFs. The summary statistics in Table 2 confirm that the leading pattern of SSTAs exhibits strong persistence through the year and from year to year: the relationships are stronger than those in Table 1 because backward, as well as forward, lag correlations are taken into account. The leading pattern of summertime SSTAs is slightly more persistent from one year to the next than the leading pattern of wintertime SSTAs. This results suggest that the summertime anomalies, which are less subject to the interannual variability forced by the ENSO cycle in the Tropics, better reflect the evolution of the coupled climate system in the North Pacific on the interdecadal timescale.

Part of the apparent disagreement between the persistence time of summertime SSTAs documented in this section and that estimated by NB can be attributed to the distinction between the autocorrelation function for SST at a fixed grid point versus the autocorrelation for an SST pattern. Figure 7 contrasts the seasonality of the autocorrelation function the leading PC of North Pacific SST (this time based on monthly data for all calendar months) with the autocorrelation functions for SST at the grid points corresponding to its primary centers of action (32°N, 159°W and 40°N, 129°W). Consistent with results of NB, the autocorrelation functions for the grid-point time series drop off rather steeply, particularly from September to the following winter. The PC exhibits generally higher autocorrelation than the local SST time series: the difference is particularly striking in the second half of the calendar year. The high values of the SCF in Tables 1 and 2 also indicate that much of the season-to-season memory of the North Pacific SST field

TABLE 2. Summary statistics for the centered SVD analyses of SSTAs over the North Pacific poleward of 18°N.

	SCF	NC	<i>r</i>
WSW	67	25	81
SWS	67	25	79
WWW	64	19	63
SSS	65	20	72

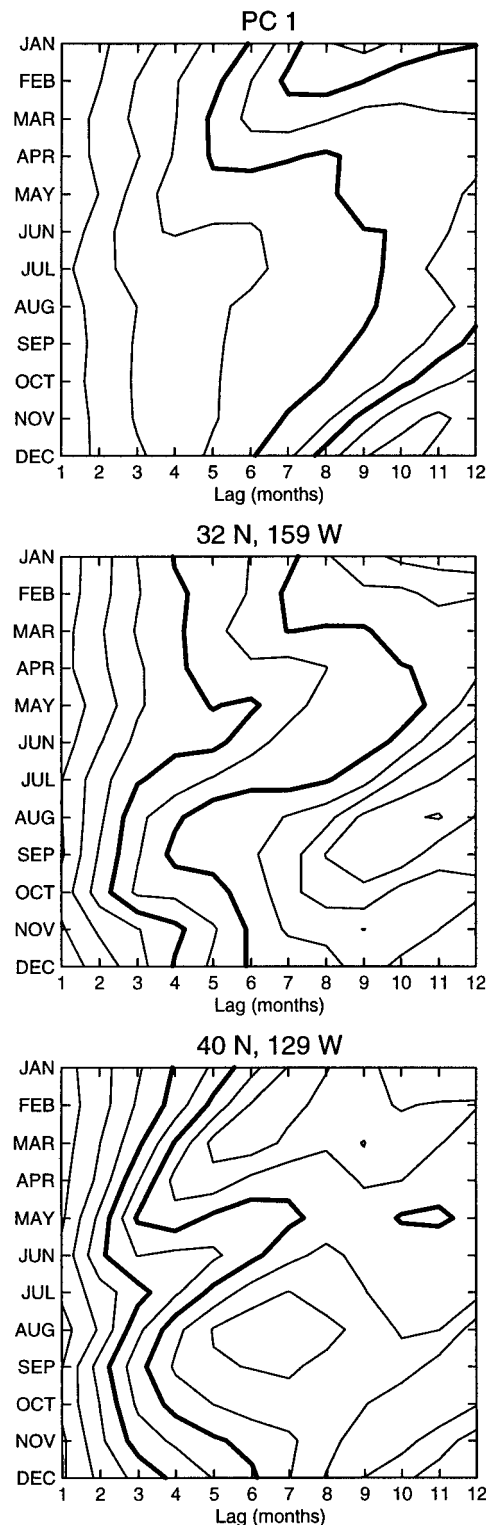


FIG. 7. Autocorrelation function based on 3-month running-mean data for the period 1950–93, starting from each calendar month for (top) the leading PC of the North Pacific SST field (corresponding to a single EOF based on data from all calendar months); (middle) SSTA for the grid box centered at 32°N, 159°W; and (bottom) SSTA for the grid box centered at 40°N, 129°W. The contour interval is 0.1; the 0.4 and 0.6 contours are thickened.

is explained by the single, seasonally varying pattern described in this paper.

#### 4. Discussion

The results presented in the previous section indicate that the dominant pattern of summertime SST over the North Pacific is at least as persistent from one year to the next as the leading wintertime EOF. Hence, it would appear that the memory of the coupled system from one winter to the next might not reside exclusively in the subsurface temperature anomalies, as might be inferred from the studies of NB and Alexander and Deser (1995). One factor that contributes to the stronger persistence of summertime SST in our results relates to the distinction between SST patterns and local SSTAs. Namias and Born (1970) interpreted their results as indicating that SST anomaly patterns are more persistent during winter than during summer, but what they actually examined was the persistence of SSTAs at fixed grid points. Our results indicate that the dominant pattern of SSTA exhibits much more persistence from summer to the next winter than the local SSTA at its primary centers of action. Just why this particular SST pattern is so much more persistent than SSTAs at fixed locations is not explained by our results.

The similarity of the leading winter and summer EOFs and the strong time continuity between their PC time series suggests that, rather than thinking of the leading EOFs of wintertime and summertime SSTAs as different modes of variability, it may be more appropriate to think of them as a single mode that undergoes a seasonal evolution. Along 40°N, the SSTAs associated with the pattern are of the same polarity year-round to the west of 140°W, but to the east of that longitude they undergo a polarity reversal between winter and summer, which detracts from the season-to-season persistence of local SSTAs at those longitudes. This distinction is evident in Fig. 7: the SST time series for the eastern Pacific grid point (lower panel) exhibits less winter-to-summer and summer-to-winter memory than the one for the central Pacific grid point (middle panel).

The seasonal polarity reversal along 40°N east of 140°W in wintertime could come about as follows. Let us suppose that at the onset of the winter season, the SSTAs along 40°N are predominantly negative. Results of some of the GCM sensitivity experiments that have been performed with extratropical SST anomalies (e.g., Ferranti et al. 1994) suggest that such cold SST anomalies in this region should tend to favor the positive polarity of the PNA pattern, whose associated latent and sensible heat fluxes should tend to reinforce the negative SSTAs to the west of 140°W. In the far eastern Pacific, the above-normal atmospheric temperature and southerly wind anomalies associated with the positive polarity of the PNA pattern should tend to warm the SST, thereby creating the wintertime pattern pictured in Figs. 1 and 4, with a node along 140°W. The relaxation of the PNA

pattern in spring would allow the SST pattern to evolve under the influence of the prevailing westerly surface winds, which would shift the node along 140°W eastward toward its summertime position. In this respect it is notable that south of the westerlies, the SSTAs in the eastern Pacific associated with the leading EOF are of the same sign year-round.

In order for SSTAs to persist through the summertime, when the mixed layer is shallow and apparently decoupled from the thermal anomalies at depth, it seems likely that some kind of positive feedback process must be operating at the air–sea interface. In a companion paper (Norris et al. 1998) we investigate the possibility that interactions involving low clouds could be functioning in this manner.

*Acknowledgments.* This work was supported by the National Science Foundation through the Climate Dynamics Program under Grant ATM 9215512 and by NASA through the Earth Observing System Program under Grant NAGW-2633.

#### REFERENCES

- Alexander, M. A., 1992: Midlatitude atmosphere–ocean interaction during El Niño. Part I: The North Pacific Ocean. *J. Climate*, **5**, 944–958.
- , and C. Deser, 1995: A mechanism for the recurrence of wintertime midlatitude SST anomalies. *J. Phys. Oceanogr.*, **25**, 122–137.
- Bottomley, M., C. K. Folland, J. Hsiung, R. E. Newell, and D. E. Parker, 1990: *Global Ocean Surface Temperature Atlas*. United Kingdom Meteorological Office, and Massachusetts Institute of Technology Department of Earth, Atmospheric and Planetary Sciences, 20 pp. and 313 maps.
- Bretherton, C. S., C. Smith, and J. M. Wallace, 1992: An intercomparison of methods for finding coupled patterns in climate data. *J. Climate*, **5**, 541–560.
- Cayan, D. R., 1992a: Latent and sensible heat flux anomalies over the northern oceans: The connection to monthly atmospheric circulation. *J. Climate*, **5**, 354–369.
- , 1992b: Latent and sensible heat flux anomalies over the northern oceans: Driving the sea surface temperature. *J. Phys. Oceanogr.*, **22**, 859–881.
- Davis, R. E., 1976: Predictability of sea surface temperature and sea level pressure anomalies over the North Pacific Ocean. *J. Phys. Oceanogr.*, **6**, 249–266.
- , 1978: Predictability of sea level pressure anomalies over the North Pacific Ocean. *J. Phys. Oceanogr.*, **8**, 233–246.
- Ferranti, L., F. Molteni, and T. N. Palmer, 1994: Impact of localized tropical and extratropical SST anomalies in ensembles of seasonal GCM integrations. *Quart. J. Roy. Meteor. Soc.*, **120**, 1613–1645.
- Fletcher, J. O., R. J. Slutz, and S. D. Woodruff, 1983: Towards a comprehensive ocean–atmosphere dataset. *Tropical Ocean Atmos. Newslett.*, **20**, 13–14.
- Frankignoul, C., 1985: Sea surface temperature anomalies, planetary waves and air–sea feedback in the middle latitudes. *Rev. Geophys.*, **23**, 357–390.
- Iwasaka, N., and J. M. Wallace, 1995: Large scale air–sea interaction in the Northern Hemisphere from a viewpoint of variations in surface heat flux by SVD analysis. *J. Meteor. Soc. Japan*, **73**, 781–794.
- Kawamura, R., 1984: Relation between atmospheric circulation and

- dominant sea-surface temperature anomaly patterns during northern winter. *J. Meteor. Soc. Japan*, **62**, 910–916.
- Kushnir, Y., and J. M. Wallace, 1989: Low-frequency variability in the Northern Hemisphere winter: Geographical distribution, structure and time-scale dependence. *J. Atmos. Sci.*, **46**, 3122–3142.
- Latif, M., and T. P. Barnett, 1994: Causes of decadal climate variability over the North Pacific/North American sector. *Science*, **226**, 634–637.
- Namias, J., 1959: Recent seasonal interactions between North Pacific waters and the overlying atmospheric circulation. *J. Geophys. Res.*, **64**, 631–646.
- , and R. M. Born, 1970: Temporal coherence in North Pacific sea-surface temperature patterns. *J. Geophys. Res.*, **75**, 5952–5955.
- Norris, J. R., Y. Zhang, and J. M. Wallace, 1998: Role of low clouds in summertime atmosphere–ocean interactions over the North Pacific. *J. Climate*, **11**, 2482–2490.
- Wallace, J. M., and Q. Jiang, 1987: On the observed structure of the interannual variability of the atmosphere–ocean climate system. *Atmospheric and Oceanic Variability*, H. Cattle, Ed., Royal Meteorological Society, 17–43.
- , Y. Zhang, and K.-H. Lau, 1993: Structure and seasonality of interannual and interdecadal variability of the geopotential height and temperature fields in the Northern Hemisphere troposphere. *J. Climate*, **6**, 2063–2082.
- Walsh, J. E., and M. B. Richman, 1981: Seasonality in the association between surface temperatures over the United States and the North Pacific Ocean. *Mon. Wea. Rev.*, **109**, 767–783.
- Yukimoto, S., M. Endoh, Y. Kitamura, A. Kitoh, T. Motoi, A. Noda, and T. Tokioka, 1996: Interannual and interdecadal variabilities in the Pacific in an MRI coupled GCM. *Climate Dyn.*, **12**, 667–683.
- Zhang, Y., J. M. Wallace, and D. S. Battisti, 1997: ENSO-like decadal variability over the Pacific sector. *J. Climate*, **10**, 1004–1020.